JARO 17: 145–158 (2016)
DOI: 10.1007/s10162-015-0549-1

JARO
Journal of the Association for Research in Otolaryngology

Research Article

Excitation Patterns of Standard and Steered Partial Tripolar Stimuli in Cochlear Implants

Ching-Chih Wu[1,2] and Xin Luo[1,3]

[1]*Department of Speech, Language, and Hearing Sciences, Purdue University, 715 Clinic Drive, West Lafayette, IN 47907, USA*
[2]*School of Electrical and Computer Engineering, Purdue University, 715 Clinic Drive, West Lafayette, IN 47907, USA*
[3]*Department of Speech and Hearing Science, Arizona State University, Coor Hall, 975 S. Myrtle Av., P. O. Box 870102, Tempe, AZ 85287, USA*

Received: 1 January 2015; Accepted: 25 November 2015; Online publication: 21 December 2015

ABSTRACT

Current steering in partial tripolar (pTP) mode has been shown to improve pitch perception and spectral resolution with cochlear implants (CIs). In this mode, a fraction (σ) of the main electrode current is returned within the cochlea and steered between the basal and apical flanking electrodes (with a proportion of α and $1-\alpha$, respectively). Pitch generally decreases when α increases from 0 to 1, although the salience of pitch change varies across CI users. This study aimed to identify the mechanism of pitch changes with pTP-mode current steering and the factors contributing to the intersubject variability in pitch-ranking sensitivity. The electrical fields were measured for steered pTP stimuli on the same main electrode with $\alpha=0$, 0.5, and 1 in five implanted ears using electrical field imaging (EFI). The related excitation patterns were also measured physiologically using evoked compound action potential (ECAP) and psychophysically using psychophysical forward masking (PFM). Consistent with the pitch-ranking results in this study, the EFI, ECAP, and PFM centroids shifted apically with increasing α. An apical shift was also observed for the PFM peak but not for the EFI or ECAP peak. The pattern width was similar with different α values within a given measure (e.g., EFI, ECAP, or PFM), but the ECAP patterns were broader than the EFI and PFM patterns, possibly because ECAP was measured with smaller σ values than EFI and PFM. The amount of pattern shift with α depended on σ (i.e., the total amount of current used for steering) but was not correlated with the pitch-ranking sensitivity across subjects. The results revealed that the pitch changes elicited by pTP-mode current steering were not only driven by the shifts of excitation centroid.

Keywords: cochlear implant, current steering, current focusing, tripolar mode, spread of excitation, forward masking pattern, electrical field imaging, compound action potential

INTRODUCTION

Profoundly deaf people may partially regain hearing sensation with the help of cochlear implants (CIs), which stimulate surviving auditory neurons using an implanted array of 10–22 electrodes. It is possible to achieve good speech recognition in quiet when temporal envelope cues in individual frequency channels are sent to the corresponding electrodes following the tonotopic organization of the cochlea (e.g., Shannon et al. 1995). In current CIs, intracochlear electrodes are most commonly stimulated in monopolar (MP) mode with current returned to a remote extracochlear electrode. The broad current spread of MP stimulation causes strong channel interaction (e.g., Chatterjee and Shannon 1998) and reduces the number of channels that provide independent cues for speech recognition (e.g., Friesen et al. 2001).

Correspondence to: Xin Luo · Department of Speech and Hearing Science · Arizona State University · Coor Hall, 975 S. Myrtle Av., P. O. Box 870102, Tempe, AZ 85287, USA. Telephone: (480) 965-9251; email: xinluo@asu.edu

Simultaneous stimulation of multiple intracochlear electrodes with well-controlled current levels and phases has been proposed to increase the spatial selectivity and spectral resolution of electrical CI stimulation. When the apical and/or basal flanking electrodes receive compensation or return current in the opposite phase to that of the middle main electrode, current spread is limited by the flanking electrodes, and excitation patterns are narrower than those of MP stimulation (e.g., Bierer 2007; Zhu et al. 2012; Landsberger et al. 2012; Saoji et al. 2013). The use of a single or both flanking return electrodes is referred to as bipolar (BP) or tripolar (TP) stimulation, respectively. The relative amount of intracochlear return current (defined as the compensation coefficient σ) ranges from 0 to 1. In human CI users, partial TP (pTP) stimulation with $\sigma < 1$ is often needed instead of full TP stimulation with $\sigma = 1$ to achieve full loudness growth within the compliance limit while keeping relatively focused excitation patterns (e.g., Mens and Berenstein 2005; Litvak et al. 2007). Compared to the traditional MP-mode CI processing strategy, a pTP-mode strategy has been shown to significantly improve speech recognition in noise for CI users (Srinivasan et al. 2013), when both strategies were matched in the channel number and stimulation rate. Improved speech recognition in noise with the pTP-mode strategy was possibly due to reduced channel interaction and increased spectral resolution.

The total intracochlear return current in pTP stimulation can be steered between the two flanking electrodes to shape the electrical field and stimulate distinct neural populations. Wu and Luo (2013) studied steered pTP stimuli on a fixed main electrode (e.g., EL8) using psychophysical pitch-ranking tests. They found that CI users generally perceived pitch lowering as the proportion of current returned to the basal flanking electrode (defined as the steering coefficient α) increased from 0 to 1. For the stimulus with $\alpha = 0$ (denoted as $pTP_{EL8,\ \alpha=0}$), all the intracochlear return current was delivered to the apical flanking electrode; for $pTP_{EL8,\ \alpha=1}$, all the intracochlear return current was delivered to the basal flanking electrode. Both cases were effectively partial BP (pBP) stimuli. Wu and Luo (2013) also used a computational model of CI stimulation to estimate the effect of α on neural excitation pattern (i.e., the number of activated neurons as a function of cochlear location). The model results showed that as α increased, the spread of excitation was attenuated on the basal side of the main electrode due to the increased basal return current, but extended on the apical side due to the reduced apical return current. Current steering between the two flanking electrodes was predicted by the model to alter the balance of apical and basal current spread without strongly affecting the excitation peak. The pitch changes perceived by CI users largely agreed with the shift of excitation centroid (i.e., center of gravity) rather than excitation peak in the model.

The pitch-ranking and model results of Wu and Luo (2013) both suggest that pTP-mode current steering can stimulate neural regions lying between adjacent standard pTP channels and thus may be useful in encoding spectral fine structure cues. However, the model-predicted mechanism of pitch changes with pTP-mode current steering due to the shift of excitation centroid needs to be verified by the excitation patterns measured in CI users. Also, in Wu and Luo (2013), CI users greatly differed in the ability to rank the steered pTP stimuli in pitch. Before the pTP-mode current steering strategy can be used clinically, it is important to understand the sources of intersubject variability in pitch-ranking performance and find measures of excitation patterns that can predict individual subjects' pitch sensitivity. To address these issues, this study measured and compared the electrical fields as well as physiological and psychophysical excitation patterns of steered pTP stimuli on main electrode EL8 with $\alpha = 0$, 0.5, and 1 in five implanted ears. Below, we will first review the different methods of excitation pattern measurements and then introduce our hypotheses based on previous pitch-ranking and model results.

Intracochlear electrical potential distribution along the electrode array can be recorded using an electrical field imaging (EFI) technique (e.g., Vanpoucke et al. 2004). The EFI patterns in individual ears are dependent on the anatomy and conductivity of cochlear tissues as well as the placement and surface properties of electrode contacts. For simultaneous stimulation of multiple electrodes, the EFI pattern can be adequately modeled by linear summation of the potential distributions of individual stimulated electrodes (e.g., Berenstein et al. 2010; Tang et al. 2011; Snel-bongers et al. 2012) and thus may change with the stimulation configuration (e.g., the α value in steered pTP mode).

Physiologically, electrically evoked compound action potential (ECAP) from a group of auditory neurons can be recorded using a forward masking subtraction technique with single stimulation pulses (e.g., Abbas et al. 1999). The spatial profile of ECAP (e.g., Cohen et al. 2003; Hughes and Abbas 2006) shows the spread of excitation for the probe by assessing the spatial and temporal interactions between the neurons activated by the masker and probe (due to the neural refractory effects). While ECAP patterns have been studied extensively for MP stimuli, those for focused TP stimuli have only been reported by Zhu et al. (2012) to be irregular with multiple

peaks. Within CI users, electrode pitch-ranking performance in MP mode has been found to be correlated with the separation of ECAP patterns between electrodes (Hughes 2008). These results motivated us to study the ECAP patterns of steered pTP stimuli to see if their separations would be correlated with the corresponding pitch-ranking performance.

Psychophysically, a forward masking technique (psychophysical forward masking—PFM; Chatterjee and Shannon 1998; Chatterjee et al. 2006) can be used to derive a masker's spread of excitation from the masker-induced elevation of probe thresholds along the electrode array. Similar to the ECAP measurement, the PFM measurement reveals the spatial and temporal interactions between the masker and probe. However, PFM is measured with pulse trains (instead of single pulses), which may lead to temporal integration and adaptation at central levels. In addition, the PFM measurement may involve psychophysical mechanisms of loudness perception at the probe threshold level. Studies have focused on comparing the width (rather than the centroid or peak) of the PFM pattern between the MP and BP or TP stimuli (e.g., Chatterjee et al. 2006; Kwon and van den Honert 2006; Landsberger et al. 2012). Saoji et al. (2013) measured the shifts of the PFM pattern from MP to pBP stimuli (also known as phantom electrode stimuli). They found that the return current in pBP stimuli pushed the centroid (and sometimes even the peak) of the PFM pattern away from the return electrode, consistent with the reported pitch changes of pBP stimuli relative to those of MP stimuli.

In this study, the EFI, ECAP, and PFM patterns would reveal the distribution of stimulation and excitation of steered pTP stimuli at different stages along the auditory pathway. Among the features of excitation pattern, we focused on analyzing the peak and centroid of excitation to verify the model-predicted pitch-change mechanism based on the shift of excitation centroid rather than peak (Wu and Luo 2013). Following the model results, our hypotheses were that the EFI and ECAP centroids would shift apically while the EFI and ECAP peaks would not change as α increased. The PFM pattern would rely on psychophysical processing of the peripheral neural responses. It is possible that both the PFM centroid and peak may shift together with α, as suggested by the results of Saoji et al. (2013). Because the degree of current focusing may affect sound quality and thus interfere with pitch perception (Mens and Berenstein 2005; Landsberger et al. 2012), we also analyzed whether the widths of EFI, ECAP, and PFM patterns would change with α. Finally, the shift of excitation centroid or peak from $\alpha = 0.5$ to $\alpha = 0$ or from $\alpha = 0.5$ to $\alpha = 1$ was hypothesized to be correlated with the corresponding pitch sensitivity measured in the pitch-ranking tests. The correlation results would indicate whether any measures used in this study can explain the intersubject variability in pitch sensitivity.

METHODS

Subjects

Four postlingually deafened CI users of the Advanced Bionics HiRes 90K implant with the HiFocus1J electrode array participated in this study. Subject demographic details can be found in Table 1. Subject S3 received bilateral CIs and her left and right implants (S3L and S3R, respectively) were both tested. This study was reviewed and approved by the Purdue IRB committee. Subjects provided informed consent and were compensated for their time.

Pitch Ranking of Steered pTP stimuli

Steered pTP stimuli on main electrode EL8 were balanced in loudness at the most comfortable level (MCL) and then ranked in pitch by each subject using the method in Wu and Luo (2013). A 10-level loudness scale from 1 (just noticeable) to 10 (too loud) designed by Advanced Bionics was used to measure loudness growth and MCL was the sixth level on this scale.[1] During the psychophysical pitch-ranking test, the highest possible compensation coefficient σ that allowed for full loudness growth within the compliance limit of the CI was used for all subjects except S4. As found in Wu and Luo (2014), S4 experienced pitch reversals between adjacent main electrodes in standard pTP mode with the highest possible σ (0.8), which may have generated perceptually salient side lobes around return electrodes. Thus, a smaller σ (0.6) was used for S4 to rank the pitches of steered pTP stimuli on EL8 in this study. The loudness of $pTP_{EL8,\ \alpha}$ with α from 0 to 1 in steps of 0.1 was balanced to that of $pTP_{EL8,\ \alpha=0.5}$ at MCL using a two-alternative, forced-choice, double-staircase procedure (Jesteadt 1980). In each trial of the pitch-ranking test, a randomly selected pair of loudness-balanced steered pTP stimuli with an α interval of 0.1 (e.g., 0.1 vs. 0.2, 0.2 vs. 0.3, etc.) were ranked in pitch. Each stimulus pair was tested 20 times, and the percentage that the stimulus with a higher α value was judged as higher in pitch was converted to a d' value (Hacker and Ratcliff 1979). Table 1 lists the pitch-ranking results from $pTP_{EL8,\ \alpha=0.5}$ to $pTP_{EL8,\ \alpha=0}$ or from $pTP_{EL8,\ \alpha=0.5}$ to $pTP_{EL8,\ \alpha=1}$ in terms of cumulative

[1] https://www.advancedbionics.com/content/dam/ab/Global/en_ce/documents/libraries/AssessmentTools/3-01203_loudness_scale-ADLT.pdf. Accessed on 28 September 2015.

TABLE 1

Demographic details, pitch-ranking sensitivity, and tested compensation coefficients of individual subjects

Subject	*Age*	*Etiology*	*Strategy*	*Years with prosthesis*	*Cumulative d′ from* $pTP_{EL8,\ \alpha=0.5}$ *to* $pTP_{EL8,\ \alpha=0}$	*Cumulative d′ from* $pTP_{EL8,\alpha=0.5}$ *to* $pTP_{EL8,\ \alpha=1}$	*σ used for pitch ranking*	*σ used for ECAP recording*
S1	85	Sudden hearing loss	HiRes-P 120	5	6.22	−5.33	0.60	0.55
S2	45	Meningitis	HiRes-P 120	9	6.06	−8.37	0.80	0.50
S3L	67	Hereditary deafness	HiRes-P	3	−0.90	−2.04	0.75	0.40
S3R	67	Hereditary deafness	HiRes-P	8	3.23	−3.19	0.65	0.55
S4	64	Unknown	HiRes-S 120	5	2.45	−0.97	0.60	0.60

d', together with the compensation coefficient σ used for each subject. The results agreed with those of Wu and Luo (2013), showing that pitch generally decreased with higher steering coefficient α. There was a large intersubject variability in the pitch sensitivity (i.e., cumulative d') to current steering in pTP mode. The electrical fields and excitation patterns of $pTP_{EL8,\ \alpha=0}$, $pTP_{EL8,\ \alpha=0.5}$, and $pTP_{EL8,\ \alpha=1}$ were thus measured for each subject to reveal the pitch-change mechanism of pTP-mode current steering and explain the variable pitch-ranking results across subjects.

EFI: Stimuli and Procedure

Intracochlear potential distributions of $pTP_{EL8,\ \alpha=0}$, $pTP_{EL8,\ \alpha=0.5}$, and $pTP_{EL8,\ \alpha=1}$ were measured using the Electrical Field Imaging and Modeling software (EFIM v1.4, Advanced Bionics, Antwerp, Belgium). The stimulus used for EFI measurement was a 2.5-ms, 3000-Hz sinusoid at a subthreshold level of 32 μA (Berenstein et al. 2010; Snel-Bongers et al. 2012). The σ value of the stimulus for each subject was the same as that in the pitch-ranking test (Table 1). For each steered pTP stimulus, electrical potentials were recorded on all the nonstimulated electrodes along the electrode array (e.g., the open diamonds in Fig. 1 for $pTP_{EL8,\ \alpha=0.5}$ in S4). The recordings on the stimulated electrodes EL7, EL8, and EL9 could not be used because they were dominated by the reactive impedance from the electrode-tissue interface rather than the resistive impedance of the cochlear tissue (e.g., Berenstein et al. 2010). To obtain the full intracochlear potential distribution of a steered pTP stimulus (e.g., $pTP_{EL8,\ \alpha=0.5}$ in S4), the electrical fields of MP stimuli on EL7, EL8, and EL9 were measured, each scaled by the corresponding current level and phase as used in the steered pTP stimulus (e.g., the upward triangles, circles, and downward triangles in Fig. 1, respectively), and then linearly summed (e.g., the black diamonds in Fig. 1). Note that for each MP stimulus, the potential on the stimulated electrode (e.g., the gray circle in Fig. 1 for MP_{EL8}) was the mean extrapolated value of two exponential curves fit to the EFI recordings (e.g., the open circles) on the apical and basal nonstimulated electrodes (e.g., EL1–7 and EL9–16), respectively (Berenstein et al. 2010). Figure 1 also shows that the linear summation of the electrical fields of individual stimulated electrodes (e.g., the black diamonds) adequately approximated the electrical field of a steered pTP stimulus (e.g., the open diamonds) on the nonstimulated electrodes (with an average percent error of 7.14 % across subjects and stimuli). This was consistent with the findings of Berenstein et al. (2010) and Tang et al. (2011). The final EFI pattern or the potential distribution of a steered pTP stimulus comprised the recorded values on the nonstimulated electrodes and the estimated values on the stimulated electrodes.

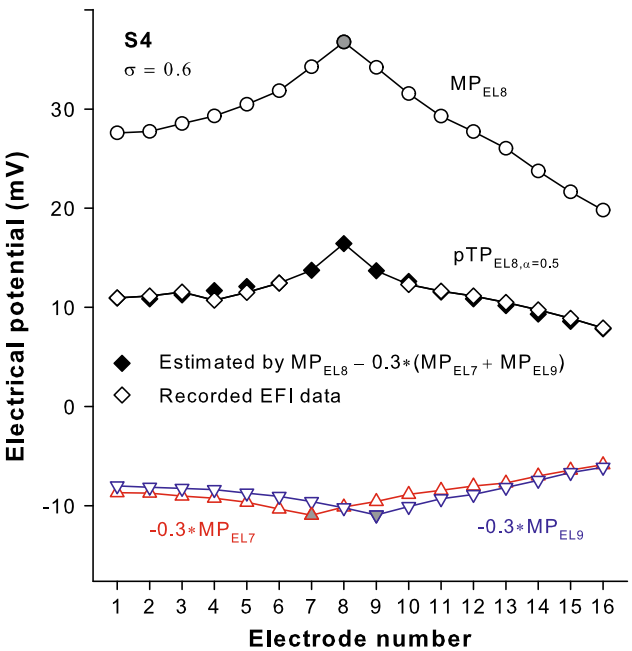

FIG. 1. Intracochlear potential distribution of $pTP_{EL8,\ \alpha=0.5}$ with $\sigma = 0.6$ in S4 recorded on the nonstimulated electrodes (*open diamonds*) and estimated on all electrodes (*black diamonds*) by adding together the potential distributions of MP_{EL8} (*circles*), $-0.3 \times MP_{EL7}$ (*upward triangles*), and $-0.3 \times MP_{EL9}$ (*downward triangles*).

ECAP: Stimuli and Procedure

ECAP for steered pTP stimuli was recorded using the Bionic Ear Data Collection System (BEDCS v1.17, Advanced Bionics, Sylmar, CA). A forward masking subtraction method (e.g., Abbas et al. 1999) was used to remove electrical stimulus artifacts while preserving neural responses. To determine the spread of neural excitation for steered pTP stimuli, the ECAP spatial profile (e.g., Cohen et al. 2003) was measured by keeping the steered pTP-mode probe on EL8 (i.e., $pTP_{EL8,\ \alpha=0}$, $pTP_{EL8,\ \alpha=0.5}$, and $pTP_{EL8,\ \alpha=1}$) while moving the MP-mode masker along the electrode array from EL1 to EL16. Both probe and masker used a biphasic cathodic-leading, charge-balanced pulse. The phase duration (32 μs) was much shorter than that used in the pitch-ranking test (226 μs) to avoid prolonged stimulus artifacts. The interval between the masker and probe pulses was 500 μs so that the neurons recruited by the masker stayed in the refractory state and did not respond to the probe. For each pair of masker and probe, the four stimulus conditions (i.e., masker and probe, masker only, probe only, and no stimulus) in the forward masking subtraction method were each repeated 128 times at a rate of 20 Hz. The sampling rate of ECAP responses was 56 kHz and the gain was 300. The ECAP responses were processed with a band-pass smoothing filter from 400 to 6000 Hz and were considered nonexisting if the estimated signal-to-noise ratio (SNR) was below 1.7 dB (Undurraga et al. 2012).

Ideally, ECAP recording should be performed at MCL as in the pitch-ranking test. However, MCL could not be reached within the compliance limit of the CI for the steered pTP-mode probe, due to the much shorter phase duration (32 μs) and slower stimulation rate (20 Hz) than those in the pitch-ranking test (226 μs and 1000 Hz, respectively). To achieve sufficient loudness for ECAP recording, the compensation coefficient σ for the steered pTP-mode probe (originally set to be the same as that in the pitch-ranking test) was reduced (Table 1) until the soft but comfortable level (which was one level below MCL on the loudness scale) could be reached. In light of the poor loudness perception of the steered pTP-mode probe, the masker was presented in MP rather than pTP mode and at MCL rather than at the soft but comfortable level. The growth of ECAP amplitude between the negative N1 and positive P2 peaks with increasing current levels for the probe $pTP_{EL8,\ \alpha=0.5}$ was measured using the MP-mode masker on EL8. The ECAP growth function confirmed that the probe $pTP_{EL8,\ \alpha=0.5}$ at the soft but comfortable level could generate reliable ECAP responses.

Figure 2 shows the example ECAP spatial profiles (i.e., the N1-P2 amplitude of ECAP response as a function of masker electrode) for $pTP_{EL8,\ \alpha=1}$ in S4. An apical and a basal recording electrode (e.g., EL7 and EL10 for $pTP_{EL8,\ \alpha=1}$) adjacent to the stimulated electrodes of the steered pTP-mode probe (e.g., EL8 and EL9 for $pTP_{EL8,\ \alpha=1}$) were both used for ECAP recording. Note that ECAP responses could not be recorded when the masker was on the recording electrode, due to amplifier saturation. As such, the ECAP spatial profile recorded from each recording electrode had a missing data point on the recording electrode (e.g., the downward and upward triangles in Fig. 2 show the spatial profiles recorded from EL7 and EL10, respectively). Averaging the ECAP spatial profiles recorded from the two recording electrodes yielded a final ECAP spatial profile without missing data (e.g., the black circles in Fig. 2). The error bars in Figure 2 represent the 95 % confidence intervals of the ECAP amplitudes measured over 128 repeats.

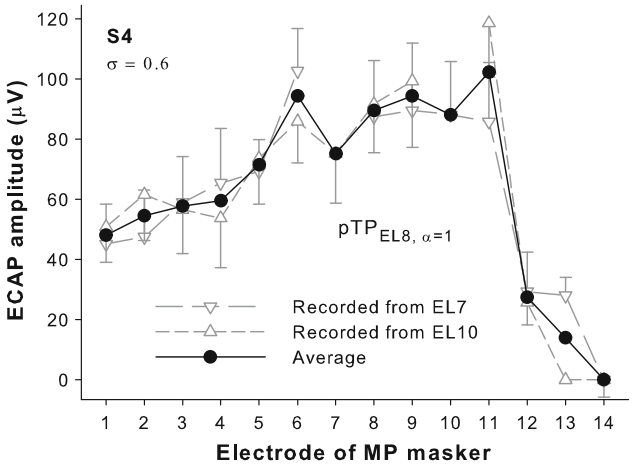

FIG. 2. ECAP amplitude as a function of masker electrode for $pTP_{EL8,\ \alpha=1}$ with $\sigma = 0.6$ in S4 recorded from EL10 (*upward triangles*) and EL7 (*downward triangles*), and then averaged (*circles*). *Error bars* represent the 95 % confidence intervals of the ECAP amplitudes measured over 128 repeats and are only shown in one direction for clarity of presentation.

PFM: Stimuli and Procedure

The excitation patterns of steered pTP stimuli were measured psychophysically using a forward masking technique (e.g., Chatterjee and Shannon 1998; Chatterjee et al. 2006; Kwon and van den Honert 2006). In this technique, thresholds of probes along the electrode array are measured with or without a forward masker. The difference between the masked and unmasked probe thresholds (i.e., the masker-induced probe threshold shift) indicates the channel interaction between the masker and probe. The probe threshold shift as a function of probe electrode may reflect the

psychophysical excitation pattern of the masker. The maskers used in this study (i.e., $pTP_{EL8,\ \alpha=0}$, $pTP_{EL8,\ \alpha=0.5}$, and $pTP_{EL8,\ \alpha=1}$ with the highest possible σ and presented at MCL) were exactly the same stimuli as those in the pitch-ranking test ("Pitch Ranking of Steered pTP Stimuli" section). The probes were standard pTP stimuli on main electrodes from EL3 to EL13 with σ fixed at 0.75 for all subjects except S1. Subject S1 could only detect probes with a smaller σ (0.65) in the presence of the forward maskers, possibly because she experienced slower psychophysical recovery and stronger masking from the maskers than younger subjects (e.g., Lee et al. 2012). Both maskers and probes were 1000-Hz, biphasic (226 μs/phase), charge-balanced, cathodic-leading pulse trains. The probes were 20 ms, while the maskers were 300 ms. The interval between the masker and probe was 10 ms. All stimuli were presented using the BEDCS.

The unmasked probe threshold was measured using a three-interval, forced-choice (3IFC), 2-down/1-up adaptive procedure. In each trial, two intervals of silence and one interval containing the probe were presented in random order. The onsets of consecutive intervals were separated by 500 ms. The color of the corresponding button on a computer screen changed to indicate the presentation of each interval, especially those of silence or with subthreshold levels. Subjects were allowed to repeat the stimuli before choosing the interval containing the probe by clicking on the corresponding button. Visual feedback was provided. The probe level was adjusted based on subject response using a 20-μA step size in the first three reversals and a 5-μA step size thereafter. Each run stopped after nine reversals, and the probe threshold was the average level across the last six reversals.

The masked probe threshold was also measured using the same 3IFC, 2-down/1-up adaptive procedure, except that in each trial, two intervals of the masker only and one interval of the masker followed by the probe were presented in random order.

Data Analysis

The spatial profile of each steered pTP stimulus measured using the EFI, ECAP, or PFM method for each subject was normalized to its peak amplitude to better compare the relative shape of stimulation or excitation patterns across α values and measurement methods. Figure 3 shows an example of the normalized ECAP pattern for $pTP_{EL8,\ \alpha=0.5}$ in S3R. The dashed horizontal line represents the normalized ECAP amplitude of 0.75. The peak location of each normalized pattern was defined as the location of the electrode with the highest normalized amplitude of 1 (e.g., EL9 in Fig. 3). As in Wu and Luo (2013), the center of gravity or the centroid of each normalized pattern was calculated as follows:

$$Centroid = \frac{\sum_k k \times |SP(k)|}{\sum_k |SP(k)|} \quad (1)$$

where k is the electrode number and $SP(k)$ is the normalized amplitude at electrode k. In Figure 3, the centroid of the ECAP pattern was 8.16 in the unit of electrode number, as indicated by the circle near the x-axis. The width at 75 % of the peak amplitude was also calculated to characterize the degree of focusing for each normalized pattern. Similar to Hughes and Abbas (2006), we also calculated the width at 75 % because it was the lowest percent of the peak amplitude where a full width could be successfully calculated for all α values, measurement methods, and subjects in this study. For the example in Figure 3, the width of the ECAP pattern was the total width of the horizontal double-arrow lines and was 9.10 in the unit of electrode spacing. All segments above 75 % of the peak amplitude (including those outside of the main exCitation area) were used in the width calculation to account for possible off-electrode listening (e.g., Dingemanse et al. 2006).

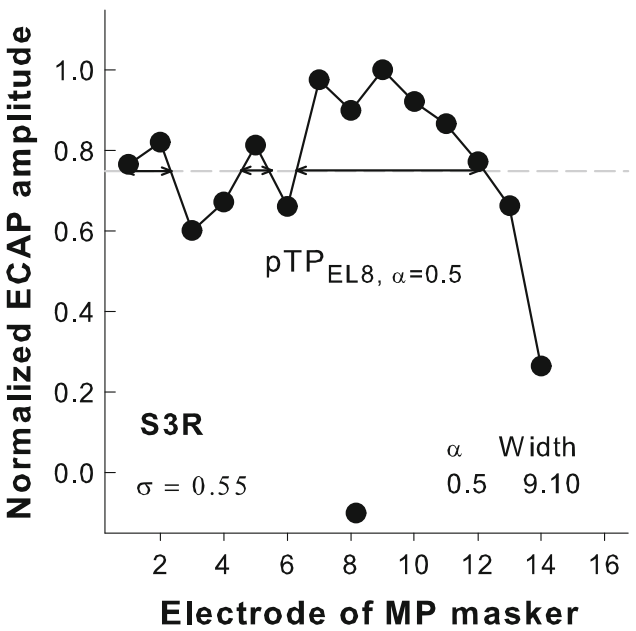

FIG. 3. An example of the normalized ECAP pattern for $pTP_{EL8,\ \alpha=0.5}$ with $\sigma=0.55$ in S3R (*connected circles*). The centroid of the ECAP pattern is indicated by a *circle* near the *x*-axis. The width at 75 % of the peak amplitude (i.e., the total width of the *horizontal double-arrow lines*) is 9.10 in the unit of electrode spacing.

RESULTS

EFI Patterns

MP Vs. Standard pTP Stimulation. Figure 4 shows the normalized EFI patterns as a function of recording electrode for the MP (open circles) and standard pTP stimuli (filled circles) on main electrode EL8 for each subject. The original unnormalized electrical potentials generated by the MP stimulation (ranging from 20 to 100 mV) were much higher than those generated by the standard pTP stimulation (ranging from 8 to 45 mV). The electrical fields of both the MP and standard pTP stimuli had a single sharp peak on EL8. The centroid of the EFI pattern (as indicated by the circles near the *x*-axis) was also around EL8 for both stimuli. The potentials fell off more quickly on both sides of the peak for the standard pTP stimulation than for the MP stimulation, suggesting that the standard pTP stimulation reduced the current spread beyond the activated electrodes. The width at 75 % of the peak amplitude of the EFI pattern (as shown in parenthesis in the unit of electrode spacing) was significantly narrower for the standard pTP stimulation than for the MP stimulation (paired *t* test: $t_4 = 3.78$, $p = 0.02$). This was similar to the results of Berenstein et al. (2010), who also found a significantly reduced EFI width as long as the σ of pTP stimulation was greater than 0.5. Although modeling studies (Bonham and Litvak 2008; Goldwyn et al. 2010) suggest that larger σ for pTP stimulation may lead to more focused or narrower distributions of electrical potentials, there was insufficient power to perform the correlation test between the width of the EFI pattern and σ across the small number of subjects in this study.

Steered pTP Stimuli. Figure 5 shows the normalized EFI patterns as a function of recording electrode for $pTP_{EL8,\ \alpha=0}$, $pTP_{EL8,\ \alpha=0.5}$, and $pTP_{EL8,\ \alpha=1}$ for each subject. The original unnormalized electrical potentials on EL8 (i.e., the peak amplitudes of the unnormalized EFI patterns) were similar for the three steered pTP stimuli within each subject, but ranged from 15 to 38 mV across subjects. It is possible that different subjects may have different cochlear conditions (e.g., fibrous tissues and bone growth), which may affect current conduction during electrical CI stimulation. The standard $pTP_{EL8,\ \alpha=0.5}$ stimulation returned the same amount of current to both flanking electrodes and thus generated roughly symmetric EFI patterns (circles) with a similar suppression of current spread on both sides of EL8. The $pTP_{EL8,\ \alpha=0}$ stimulation injected the intracochlear return current completely to the apical flanking electrode EL7, and thus, the electrical potentials (upward triangles) were strongly reduced on the apical side (i.e., EL1–EL7) but not on the basal side (i.e., EL9–EL16). For S2, S3L, and S3R, the large amount of current returned to EL7 (due to the large σ values) even resulted in a strong dip of the EFI pattern on EL7. Compared to $pTP_{EL8,\ \alpha=0}$, $pTP_{EL8,\ \alpha=1}$ generated reversed EFI patterns (downward triangles), which were strongly attenuated on the basal side (i.e., EL9–EL16) but not on the apical side (i.e., EL1–EL7).

On average, the centroid of the EFI pattern shifted apically as α increased ($pTP_{EL8,\ \alpha=0}$: 8.55, $pTP_{EL8,\ \alpha=0.5}$: 8.00, and $pTP_{EL8,\ \alpha=1}$: 7.37, as shown by the corresponding symbols near the *x*-axis). A one-way repeated-measures (RM) analysis of variance (ANOVA) showed a significant effect of α value on the EFI centroid location ($F_{2,\ 8} = 7.59$, $p = 0.01$). Post hoc pairwise comparisons using the Holm-Sidak method showed that the centroid location was significantly more basal for $pTP_{EL8,\ \alpha=0}$ than for $pTP_{EL8,\ \alpha=1}$ ($p = 0.01$), but was not significantly different between any other pair of the steered pTP stimuli ($p > 0.11$). The width at 75 % of the peak amplitude of the EFI pattern was narrower for $pTP_{EL8,\ \alpha=0.5}$ than for $pTP_{EL8,\ \alpha=0}$ and $pTP_{EL8,\ \alpha=1}$ (on average, 1.88, 2.44, and 2.56 in the unit of electrode spacing, respectively). A one-way RM ANOVA showed that the effect of α

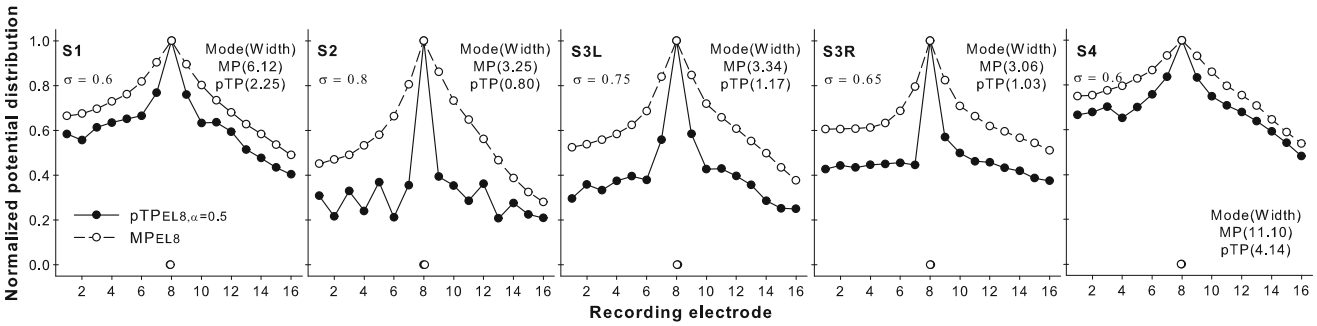

FIG. 4. Normalized EFI patterns as a function of recording electrode for the MP (*open circles*) and standard pTP stimuli (*filled circles*) on main electrode EL8 for each subject. The centroid of each pattern is indicated by the corresponding symbol near the *x*-axis. The width at 75 % of the peak amplitude of each pattern is shown in the parenthesis in the unit of electrode spacing.

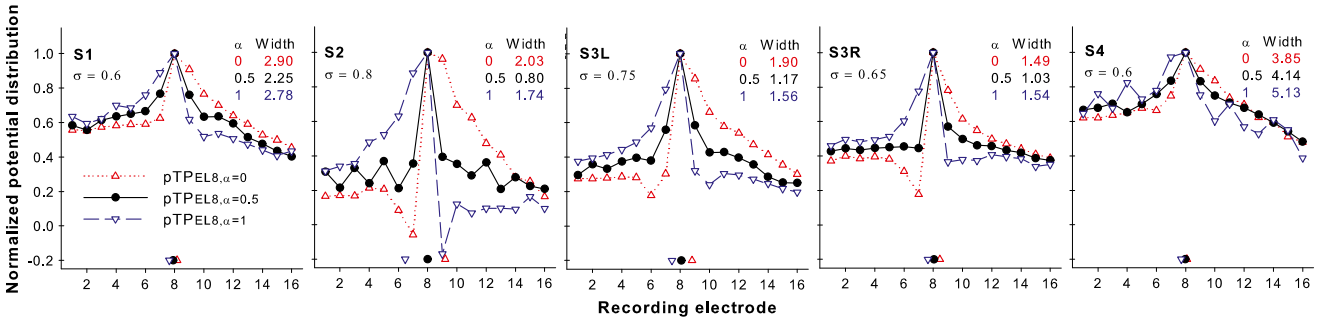

FIG. 5. Normalized EFI patterns as a function of recording electrode for $pTP_{EL8,\ \alpha=0}$ (*upward triangles*), $pTP_{EL8,\ \alpha=0.5}$ (*circles*), and $pTP_{EL8,\ \alpha=1}$ (*downward triangles*) for each subject. The centroid of each pattern is indicated by the corresponding symbol near the *x*-axis. The width at 75 % of the peak amplitude of each pattern is shown in the unit of electrode spacing.

value on the width of the EFI pattern was of borderline significance ($F_{2,\ 8}=4.74$, $p=0.04$). Post hoc pairwise comparisons showed that there was no significant difference in the EFI width between any pair of the steered pTP stimuli, although the width difference between $pTP_{EL8,\ \alpha=0.5}$ and $pTP_{EL8,\ \alpha=1}$ approached significance ($p=0.06$).

ECAP Patterns

Figure 6 shows the normalized ECAP patterns for the probes $pTP_{EL8,\ \alpha=0}$ (upward triangles), $pTP_{EL8,\ \alpha=0.5}$ (circles), and $pTP_{EL8,\ \alpha=1}$ (downward triangles) as a function of masker electrode for each subject. S2 showed much larger original unnormalized ECAP amplitudes than the other subjects, possibly because she was much younger and had used CI for more years, although meningitis may have led to poorer neural survival for her (Hinojosa and Marion 1983). For the bilateral CI user S3, the original ECAP responses of her first CI (S3R) were stronger with higher SNRs than those of her second CI (S3L), likely due to better neural survival in her first implanted ear with a shorter duration of deafness. The neural responses to steered pTP stimuli were weak (e.g., 70–130 μV with the MP-mode masker on EL8) and prone to the influence of electrical stimulus artifacts during ECAP recording. The low SNRs in ECAP recording led to irregular changes (e.g., those on the apical electrodes in S3R) or zero values of the ECAP amplitudes (e.g., those on the apical/basal electrodes in S3L). For subjects with larger σ values (e.g., S4, S1, and S3R), there was a trend that, as α increased, the normalized ECAP amplitudes slightly increased on the apical side of EL8 but decreased on the basal side of EL8. On average, the peak location of the ECAP pattern shifted basally as α increased ($pTP_{EL8,\ \alpha=0}$: 8.4, $pTP_{EL8,\ \alpha=0.5}$: 8.6, and $pTP_{EL8,\ \alpha=1}$: 9.4). However, it was difficult to identify a single prominent peak for each ECAP pattern. Also, a one-way RM ANOVA showed that the changes in the ECAP peak location with α were not significant ($F_{2,\ 8}=2.15$, $p=0.18$). The centroid location of the ECAP pattern was estimated for each steered pTP probe (as shown by the corresponding symbol near the *x*-axis). On average, the centroid location of the ECAP pattern shifted apically as α increased ($pTP_{EL8,\ \alpha=0}$: 8.07, $pTP_{EL8,\ \alpha=0.5}$: 7.72, and $pTP_{EL8,\ \alpha=1}$: 7.51). Thus, the ECAP centroid and peak moved with α in the opposite directions. Due to the violation of the normality assumption, a Friedman RM ANOVA on ranks was used to analyze the ECAP centroids and showed a significant effect of α value ($\chi^2=8.40$, $p=0.01$). Post hoc pairwise comparisons using the Tukey method

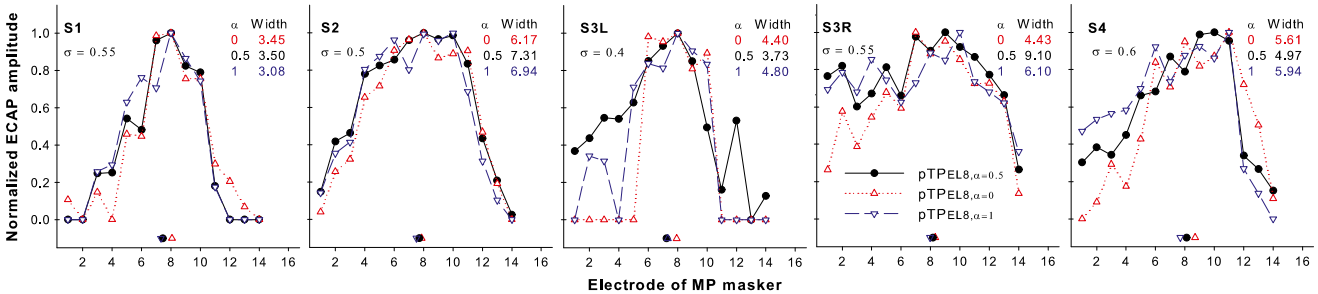

FIG. 6. Normalized ECAP patterns as a function of masker electrode for $pTP_{EL8,\ \alpha=0}$ (*upward triangles*), $pTP_{EL8,\ \alpha=0.5}$ (*circles*), and $pTP_{EL8,\ \alpha=1}$ (*downward triangles*) for each subject. The centroid of each pattern is indicated by the corresponding symbol near the *x*-axis. The width at 75 % of the peak amplitude of each pattern is shown in the unit of electrode spacing.

showed that the location of the ECAP centroid was significantly more basal for $pTP_{EL8,\ \alpha=0}$ than for $pTP_{EL8,\ \alpha=1}$ ($p<0.05$), but was not significantly different between any other pair of the steered pTP probes ($p>0.05$). The width at 75 % of the peak amplitude of the ECAP pattern did not significantly change with α (on average, $pTP_{EL8,\ \alpha=0}$: 4.81, $pTP_{EL8,\ \alpha=0.5}$: 5.72, and $pTP_{EL8,\ \alpha=1}$: 5.37 in the unit of electrode spacing) (one-way RM ANOVA: $F_{2,\ 8}=0.77$, $p=0.49$).

PFM Patterns

Figure 7 shows the normalized threshold shifts of pTP probes (i.e., the differences in dB between the masked and unmasked probe thresholds) with the forward maskers $pTP_{EL8,\ \alpha=0}$ (upward triangles), $pTP_{EL8,\ \alpha=0.5}$ (circles), and $pTP_{EL8,\ \alpha=1}$ (downward triangles) as a function of probe electrode for each subject. The normalized PFM patterns mostly had a single peak and decreased monotonically toward the apex and base when the probe moved away from the masker. For all subjects, the PFM patterns gradually shifted from base to apex as α increased. Although the three steered pTP maskers had the same main electrode EL8, current steering between the flanking electrodes shifted the PFM peak for all subjects except S3R. The PFM peak location was on average 9.2, 7.8, and 6.6 for $pTP_{EL8,\ \alpha=0}$, $pTP_{EL8,\ \alpha=0.5}$, and $pTP_{EL8,\ \alpha=1}$, respectively. A one-way RM ANOVA showed a significant effect of α value on the PFM peak location ($F_{2,\ 8}=6.96$, $p=0.02$). Post hoc pairwise comparisons using the Holm-Sidak method showed that the PFM peak location was significantly more basal for $pTP_{EL8,\ \alpha=0}$ than for $pTP_{EL8,\ \alpha=1}$ ($p=0.02$), but was not significantly different between any other pair of the steered pTP maskers ($p>0.12$). The centroid of each PFM pattern was shown by the corresponding symbol near the *x*-axis. On average, the PFM centroid also shifted from base to apex as α increased ($pTP_{EL8,\ \alpha=0}$: 8.76, $pTP_{EL8,\ \alpha=0.5}$: 7.60, and $pTP_{EL8,\ \alpha=1}$: 6.74). A one-way RM ANOVA showed a significant effect of α value on the PFM centroid location ($F_{2,\ 8}=17.92$, $p=0.001$). Post hoc pairwise comparisons using the Holm-Sidak method showed significantly different PFM centroid locations between $pTP_{EL8,\ \alpha=0}$ and $pTP_{EL8,\ \alpha=0.5}$ ($p=0.02$) and between $pTP_{EL8,\ \alpha=0.5}$ and $pTP_{EL8,\ \alpha=1}$ ($p=0.03$). The width at 75 % of the peak amplitude of the PFM pattern was on average 4.02, 3.28, and 3.86 in the unit of electrode spacing for $pTP_{EL8,\ \alpha=0}$, $pTP_{EL8,\ \alpha=0.5}$, and $pTP_{EL8,\ \alpha=1}$, respectively. No significant effect of α value was found on the PFM width (one-way RM ANOVA: $F_{2,\ 8}=1.70$, $p=0.24$).

Comparisons Across Measurement Methods

Figure 8 shows the peak, centroid, and width of the EFI, ECAP, and PFM patterns as a function of α for the steered pTP stimuli. To investigate how the spatial profiles of steered pTP stimuli varied across the different measurements, the pattern peak, centroid, and width were analyzed by separate two-way RM ANOVAs with measurement method and α value as the two factors, followed by the Holm-Sidak post hoc *t* tests.

For the pattern peak, there were no significant effects of α value ($F_{2,\ 16}=1.24$, $p=0.34$) and measurement method ($F_{2,\ 16}=2.67$, $p=0.13$), but the interaction between the two factors was significant ($F_{4,\ 16}=9.33$, $p<0.001$). The significant interaction reflected the fact that the EFI and ECAP peaks had no significant movements, while the PFM peak shifted from base to apex with increasing α (as described in previous sections). Post hoc *t* tests showed that the peak locations of $pTP_{EL8,\ \alpha=0}$ and $pTP_{EL8,\ \alpha=0.5}$ did not vary across measurement methods, while that of $pTP_{EL8,\ \alpha=1}$ was significantly different between any two measurement methods ($p<0.05$).

For the pattern centroid, there was no significant effect of measurement method ($F_{2,\ 16}=1.51$, $p=0.28$). However, the effect of α value ($F_{2,\ 16}=20.96$, $p<0.001$) and the interaction between the two factors ($F_{4,\ 16}=5.04$, $p=0.008$) were both significant. The significant interaction was driven by the greater shifts of the PFM centroid than the EFI and ECAP centroids with increasing α (as described in previous sections). Post hoc *t* tests showed that the centroid locations of $pTP_{EL8,\ \alpha=0}$ and $pTP_{EL8,\ \alpha=0.5}$ did not vary across

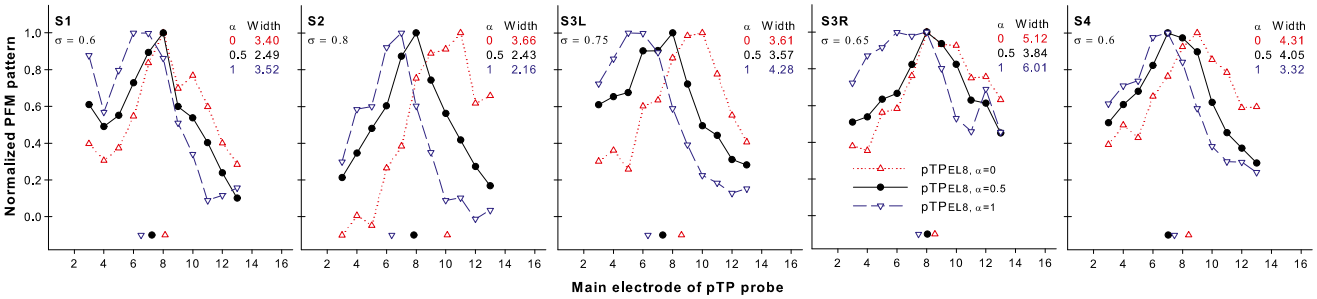

FIG. 7. Normalized PFM patterns as a function of probe electrode for $pTP_{EL8,\ \alpha=0}$ (*upward triangles*), $pTP_{EL8,\ \alpha=0.5}$ (*circles*), and $pTP_{EL8,\ \alpha=1}$ (*downward triangles*) for each subject. The centroid of each pattern is indicated by the corresponding symbol near the *x*-axis. The width at 75 % of the peak amplitude of each pattern is shown in the unit of electrode spacing.

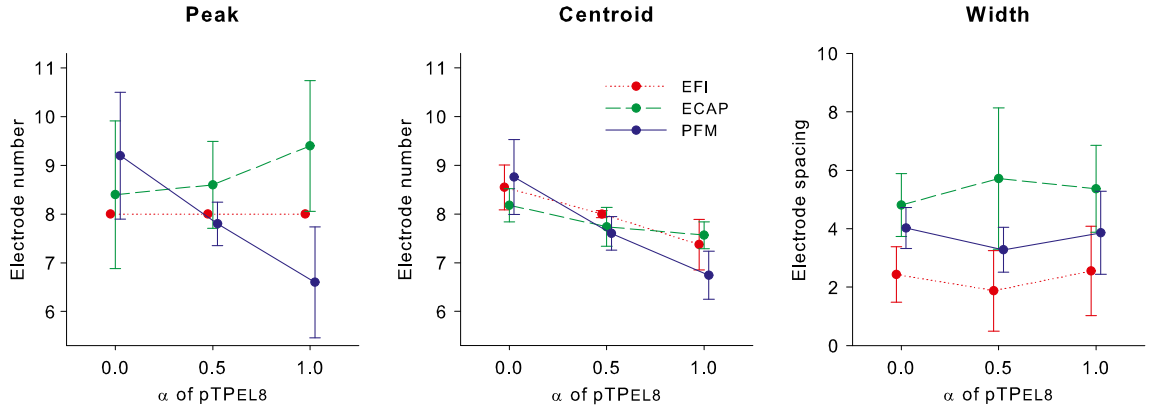

FIG. 8. Peak (*left panel*), centroid (*middle panel*), and width (*right panel*) of the EFI, ECAP, and PFM patterns as a function of α for the steered pTP stimuli on main electrode EL8.

measurement methods, while the PFM centroid location of $pTP_{EL8,\ \alpha=1}$ was significantly more apical than its EFI and ECAP centroid locations ($p<0.03$).

The pattern width was similar with different α values within a given measure but varied across measurement methods (i.e., in the descending order: ECAP, PFM, and EFI widths). There was a significant effect of measurement method ($F_{2,\ 16}=7.14$, $p=0.02$), but not of α value ($F_{2,\ 16}=0.96$, $p=0.42$) or their interaction ($F_{4,\ 16}=1.33$, $p=0.30$). Post hoc t tests showed that the width was significantly different between the ECAP and EFI patterns ($p=0.02$), but was similar between the ECAP and PFM patterns or between the PFM and EFI patterns ($p>0.11$).

Correlation Between Pitch-Ranking Sensitivity and Excitation Pattern Shift

The cumulative d' of pitch ranking from $pTP_{EL8,\ \alpha=0.5}$ to $pTP_{EL8,\ \alpha=0}$ or from $pTP_{EL8,\ \alpha=0.5}$ to $pTP_{EL8,\ \alpha=1}$ is listed in Table 1. The cumulative d' values were usually positive from $pTP_{EL8,\ \alpha=0.5}$ to $pTP_{EL8,\ \alpha=0}$ and negative from $pTP_{EL8,\ \alpha=0.5}$ to $pTP_{EL8,\ \alpha=1}$. That means $pTP_{EL8,\ \alpha=0}$ was generally higher in pitch than $pTP_{EL8,\ \alpha=0.5}$, while $pTP_{EL8,\ \alpha=1}$ was lower in pitch than $pTP_{EL8,\ \alpha=0.5}$. This pitch lowering from $\alpha=0$ to $\alpha=0.5$ and then to $\alpha=1$ was consistent with the significant apical shifts of the EFI centroid, PFM centroid, and PFM peak (as presented in previous sections). Figure 9 shows the cumulative d' from $pTP_{EL8,\ \alpha=0.5}$ to $pTP_{EL8,\ \alpha=0}$ (in red) or to $pTP_{EL8,\ \alpha=1}$ (in blue) as a function of the corresponding shift of the EFI centroid (left panel), PFM centroid (middle panel), or PFM peak (right panel) for individual subjects. Apical shifts were represented as negative values, while basal shifts as positive values. Across subjects, the cumulative d' from $pTP_{EL8,\ \alpha=0.5}$ to either $pTP_{EL8,\ \alpha=0}$ or $pTP_{EL8,\ \alpha=1}$ was not correlated with the shift of the EFI centroid, PFM centroid, or PFM peak (see the first two rows of the figure legends). This suggests that the intersubject variability in pitch-ranking sensitivity with pTP-mode current steering cannot be predicted

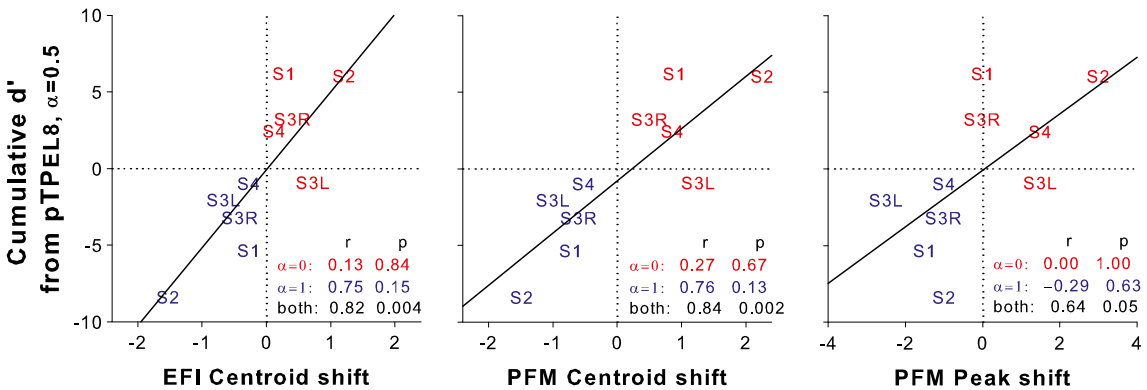

FIG. 9. Cumulative d' from $pTP_{EL8,\ \alpha=0.5}$ to $pTP_{EL8,\ \alpha=0}$ (*in red*) or to $pTP_{EL8,\ \alpha=1}$ (*in blue*) as a function of the corresponding EFI centroid shift (*left panel*), PFM centroid shift (*middle panel*), and PFM peak shift (*right panel*). The *solid lines* indicate the linear regression between the pitch-ranking sensitivity and pattern shift for both $pTP_{EL8,\ \alpha=0}$ and $pTP_{EL8,\ \alpha=1}$.

by the measures of stimulation or excitation pattern shift. When the data for both $pTP_{EL8,\ \alpha=0}$ and $pTP_{EL8,\ \alpha=1}$ were included in the Pearson correlation analyses, the cumulative d' was significantly correlated with the EFI and PFM centroid shifts and marginally correlated with the PFM peak shift (see the third row of the figure legends). These correlations, however, were driven by the opposite directions of both pitch change and pattern shift for $pTP_{EL8,\ \alpha=0}$ and $pTP_{EL8,\ \alpha=1}$, rather than by the different degrees of pitch change and pattern shift for individual subjects.

It is possible that the pitch-ranking sensitivity may depend on both the shift and width of the stimulation or excitation pattern. For example, the same amount of pattern shift may lead to better pitch-ranking sensitivity if the pattern is narrower in width. The shifts of the EFI centroid, PFM centroid, and PFM peak from $pTP_{EL8,\ \alpha=0.5}$ to $pTP_{EL8,\ \alpha=0}$ or to $pTP_{EL8,\ \alpha=1}$ were thus divided by the average width of the two involved patterns to derive a better predictor for pitch-ranking sensitivity. However, the pattern shifts relative to the pattern width were still uncorrelated with the cumulative d' of pitch ranking for either $pTP_{EL8,\ \alpha=0}$ or $pTP_{EL8,\ \alpha=1}$ across subjects.

DISCUSSION

This study investigated the electrical fields and excitation patterns of steered pTP stimuli measured by EFI, ECAP, and PFM. The pattern centroid shifted apically with increasing α in steered pTP stimuli for all the measurements, consistent with the pitch lowering observed in the pitch-ranking tests and the model results in Wu and Luo (2013). The pattern peak shifted in the same direction only for the PFM patterns, but not for the EFI or ECAP patterns. However, the shift of pattern centroid or peak was not correlated with the pitch-ranking sensitivity across subjects. The patterns were similarly wide with different α values within a given measure but were wider as measured by ECAP than by EFI and PFM, most likely because the ECAP recording used smaller σ values than the EFI and PFM testing. These results provided useful insights into the effects of pTP-mode current steering on the stimulation and excitation patterns along the auditory pathway.

Current Steering with Steered pTP Stimuli

The effects of pTP-mode current steering on the stimulation and excitation patterns were different with different measurement methods. The EFI peak did not move while the EFI centroid shifted apically with increasing α. These effects resulted from the linear summation of the electrical fields of EL7, EL8, and EL9 involved in the steered pTP stimuli. As α increased, the negative electrical field of the basal return electrode EL9 (e.g., downward triangles in Fig. 1) increased, while that of the apical return electrode EL7 (e.g., upward triangles in Fig. 1) decreased. The electrical field of the main electrode EL8 (e.g., circles in Fig. 1) thus had more reduction on the basal side than on the apical side, resulting in apically shifted EFI centroid. In contrast, the highest electrical potential remained on EL8 after the linear summation of the electrical fields. Different subjects had different degrees of EFI centroid shift from $\alpha=0.5$ to $\alpha=0$ or 1, which may be attributed to the subject-specific σ value (i.e., the total amount of current steered between the two flanking electrodes). Additional correlation analyses showed that across subjects, Pearson correlations were significant between the EFI centroid shifts and σ ($r=0.97$, $p=0.006$ for $\alpha=0$; $r=0.91$, $p=0.03$ for $\alpha=1$).

Physiologically, the ECAP peak slightly shifted basally while the ECAP centroid significantly shifted apically with increasing α. When α was 0 or 1, relatively high ECAP amplitudes were sometimes observed around the single return electrode (i.e., EL7 for $\alpha=0$ and EL9 for $\alpha=1$), although it was unlikely to have side-lobe effects (e.g., Litvak et al. 2007) with the small σ values used for ECAP recording. Further away from the main and return electrodes, the ECAP amplitudes were instead lower on the side of the single return electrode than on the other side. This caused the ECAP centroid to shift in the opposite direction as the ECAP peak with increasing α. Compared to the EFI and PFM centroids, the ECAP centroid shifted in the same direction but to a lesser degree as α increased. This may be because the smaller σ values used for ECAP recording limited the amount of current steered between the flanking electrodes and reduced the effect of pTP-mode current steering on the ECAP pattern. For a similar reason, additional correlation analyses revealed that the small σ value was not correlated with the generally small amount of ECAP centroid shift from $\alpha=0.5$ to $\alpha=0$ or 1 (Pearson correlations: $r=0.20$, $p=0.75$ and $r=0.73$, $p=0.16$, respectively).

Psychophysically, both the PFM peak and centroid significantly shifted apically as α increased. Several studies (Zhu et al. 2012; Landsberger et al. 2012; Saoji et al. 2013) have recently measured the psychophysical spatial tuning curves and forward masking patterns for (partial or full) BP and TP stimuli. In Zhu et al. (2012), the tip of spatial tuning and the peak of forward masking for full TP stimulation were shifted or split, possibly due to a dead region or poor neural

survival around the main electrode. However, the PFM patterns of standard pTP stimulation with $\alpha=0.5$ in this study had a single peak on the main electrode EL8, suggesting that there was unlikely a dead region around EL8 for our subjects. Saoji et al. (2013) found that relative to MP stimulation, pBP stimulation with an apical return electrode (similar to pTP stimulation with $\alpha=0$ in this study) had a basally shifted PFM centroid, while pBP stimulation with a basal return electrode (similar to pTP stimulation with $\alpha=1$ in this study) had an apically shifted PFM centroid. These PFM centroid shifts were in the same directions but smaller (~0.5 electrode spacing) than those in this study (~1 electrode spacing), possibly because σ was smaller (0.5) in Saoji et al. (2013). Borderline or significant Pearson correlations were found in additional correlation analyses between the σ value and PFM centroid shifts in this study ($r=0.84$, $p=0.08$ for $\alpha=0$; $r=0.92$, $p=0.03$ for $\alpha=1$). The PFM centroid shifts of ~1 electrode spacing from $\alpha=0.5$ to $\alpha=0$ or 1 in this study were consistent with the results of pitch ranking between steered pTP stimuli on adjacent main electrodes in Wu and Luo (2013). For example, Wu and Luo (2013) found that $pTP_{EL8,\ \alpha=1}$ and $pTP_{EL7,\ \alpha=0.5}$ were similar in pitch and thus may have a similar excitation centroid. As such, the excitation centroid of $pTP_{EL8,\ \alpha=1}$ (similar to that of $pTP_{EL7,\ \alpha=0.5}$) should be ~1 electrode spacing apical to that of $pTP_{EL8,\ \alpha=0.5}$.

Significant shifts of pattern peak in the same directions as those of pattern centroid were only found for the PFM patterns but not for the EFI or ECAP patterns. The PFM peak shifts were thus the results of central processing beyond the electrode-neuron interface. A psychophysical mechanism that may account for the PFM peak shifts is the off-electrode listening in electric hearing (Dingemanse et al. 2006), analogous to the off-frequency listening in acoustic hearing (Patterson 1976). For $pTP_{EL8,\ \alpha=0}$ and $pTP_{EL8,\ \alpha=1}$, the largest amount of PFM was not on EL8 (Fig. 7) where the peak electrical potential was located, suggesting that subjects may have attended to the responses of neurons far from EL8 to detect the probe. The largest amount of PFM and the minimum contribution of off-electrode listening may be found around the geometric center rather than the peak of the EFI pattern. Such central processing that takes into account information from all spectral channels may have also led to the greater PFM centroid shifts than the EFI or ECAP centroid shifts with pTP-mode current steering.

Stimulation and Excitation Widths of Steered pTP Stimuli

The present results showed that regardless of the measurement methods, steered pTP stimuli with $\alpha=0$, 0.5, and 1 had similarly wide spatial profiles. Therefore, the pitch changes with pTP-mode current steering were not due to different degrees of current focusing. The steered pTP maskers $pTP_{EL8,\ \alpha=0}$, $pTP_{EL8,\ \alpha=0.5}$, and $pTP_{EL8,\ \alpha=1}$ used in the PFM testing had similar MCL levels (additional one-way RM ANOVA: $F_{2,\ 8}=3.28$, $p=0.09$), in line with their similar excitation widths. Steered pTP stimulation with $\alpha=0$ or 1 is effectively pBP stimulation with a single apical or basal return electrode, respectively. Previous studies mostly compared the excitation width of pBP or pTP stimulation with that of MP stimulation (e.g., Saoji et al. 2013; Landsberger et al. 2012). Only one study (Zhu et al. 2012) directly compared the excitation width between full BP and TP stimuli. Similar to the present results, the width of spatial tuning curve was not significantly different between full BP and TP stimuli in Zhu et al. (2012). It seems that the degree of current focusing may rely on the total amount of intracochlear return current, regardless of the distribution of return current between the flanking electrodes.

The spatial profiles of steered pTP stimuli with $\alpha=0$, 0.5, and 1 were wider as measured by ECAP than by EFI or PFM. In our pilot study, the ECAP responses could only be reliably recorded for σ values smaller than those used in the EFI or PFM testing, which may be the main reason for less focused physiological excitation patterns. Studies (e.g., Landsberger et al. 2012) suggest that σ needs to be greater than 0.75 to generate significantly more focused pTP excitation patterns than MP excitation patterns. Note that S4 was tested with the same σ value of 0.6 in different measurement methods. However, her ECAP patterns were still wider than her EFI or PFM patterns, suggesting that factors other than σ may have also contributed to the broader spread of ECAP responses. Recall that the PFM patterns of steered pTP maskers were measured with focused standard pTP probes at threshold levels, while the ECAP patterns of steered pTP probes were measured with broad MP maskers at MCL along the electrode array. The different masker-probe configurations may also partially explain the larger excitation width measured by ECAP.

No Correlation Between Pitch-Ranking Sensitivity and Excitation Pattern Shift

For pTP-mode current steering, while the direction of excitation pattern shift was consistent with the direction of perceived pitch change, the amount of excitation pattern shift could not predict each subject's pitch-ranking sensitivity. The correlation between the amount of excitation pattern shift and the

cumulative d' of pitch ranking was weak even when the excitation pattern and pitch ranking were measured psychophysically for the same steered pTP stimuli. In addition to the small number of subjects, the different natures and methods of pitch ranking and excitation pattern measurements may have also weakened the correlation. For example, pitch ranking was tested with ±0.5-dB amplitude roving so that subjects had to separate loudness variations from pitch changes, while the PFM patterns were measured for fixed-level maskers. The pitch-ranking sensitivity was quantified as the summation of d' values between steered pTP stimuli with an α interval of 0.1, while the PFM pattern shift was directly calculated between steered pTP stimuli with an α interval of 0.5 (i.e., $\alpha=0.5$ vs. $\alpha=0$ or $\alpha=1$). For subjects with poorer pitch-ranking sensitivity, the α interval of 0.1 used for pitch ranking may not be big enough to reliably measure the d' values (Wu and Luo 2013). Also, the excitation pattern shift may better predict the ability to discriminate rather than rank the steered pTP stimuli in pitch. Another reason for the weak correlations is that pitch ranking could involve a lot more factors (e.g., the duration of deafness, listening experience, and cognitive function) than the electrical potential distribution or the excitability of peripheral neurons. For example, S1 had the most extensive musical experience among the subjects, which may explain her better pitch-ranking performance with similar excitation pattern shifts than those of S3 and S4.

Implications for Future Studies

The EFI, ECAP, and PFM patterns of $pTP_{EL8,\ \alpha=0}$, $pTP_{EL8,\ \alpha=0.5}$, and $pTP_{EL8,\ \alpha=1}$ measured in this study revealed the underlying mechanism of pitch changes elicited by pTP-mode current steering and the responses to steered pTP stimuli at different stages of the auditory pathway. Considering the great potential of pTP-mode current steering in generating additional distinctive spectral channels, future studies should implement this novel strategy of combining current steering and current focusing in a real-time, multichannel CI processor and investigate its benefits to speech and music perception with CIs. Correlation analyses should be conducted to check if the pitch-ranking sensitivity and excitation pattern shift measured in this study may be predictive of the speech and music performance with pTP-mode current steering. On the other hand, this study highlighted the challenge of measuring the growth function and spatial profile of ECAP responses to focused pTP stimuli. It was learned that ECAP recording was unreliable with the highest possible σ value that supported full loudness growth within the compliance limit (i.e., the σ value used in EFI and PFM testing). Instead, ECAP responses had to be recorded with a smaller σ value, which may reduce the effects of pTP-mode current focusing and steering on the ECAP pattern. This methodological pitfall also made it difficult to compare the spatial profiles across measurement methods. Because ECAP thresholds are important objective measures used to facilitate the CI programming in clinical cases with limited behavioral data, future studies should find ways to reliably measure the ECAP responses to pTP stimuli that typically use high σ values and long phase durations.

ACKNOWLEDGMENTS

We are grateful to all subjects for their participation in the experiments. We thank Carlo Berenstein and Filiep Vanpoucke for providing the software and technical support for EFI recording. We thank Leo Litvak for his helpful discussions on ECAP recording and Jaime Undurraga for providing the MATLAB code for ECAP processing. Research was supported in part by NIH (R21-DC-011844).

REFERENCES

Abbas PJ, Brown CJ, Shallop JK, Firszt JB, Hughes ML, Hong SH, Staller SJ (1999) Summary of results using the Nucleus CI24M implant to record the electrically evoked compound action potential. Ear Hear 20:45–59

Berenstein CK, Vanpoucke FJ, Mulder JJ, Mens LH (2010) Electrical field imaging as a means to predict the loudness of monopolar and tripolar stimuli in cochlear implant patients. Hear Res 270:28–38

Bierer JA (2007) Threshold and channel interaction in cochlear implant users: Evaluation of the tripolar electrode configuration. J Acoust Soc Am 121:1642–1653

Bonham BH, Litvak LM (2008) Current focusing and steering: modeling, physiology, and psychophysics. Hear Res 242:141–153

Chatterjee M, Shannon RV (1998) Forward masked excitation patterns in multielectrode electrical stimulation. J Acoust Soc Am 103:2565–2572

Chatterjee M, Galvin JJ, Fu QJ, Shannon RV (2006) Effects of stimulation mode, level and location on forward-masked excitation patterns in cochlear implant patients. J Assoc Res Otolaryngol 7:15–25

Cohen LT, Richardson LM, Saunders E, Cowan RSC (2003) Spatial spread of neural excitation in cochlear implant recipients: comparison of improved ECAP method and psychophysical forward masking. Hear Res 179:72–87

Dingemanse JG, Frijns JH, Briaire JJ (2006) Psychophysical assessment of spatial spread of excitation in electrical hearing with single and dual electrode contact maskers. Ear Hear 27:645–657

Friesen LM, Shannon RV, Baskent D, Wang X (2001) Speech recognition in noise as a function of the number of spectral channels: comparison of acoustic hearing and cochlear implants. J Acoust Soc Am 110:1150–1163

Goldwyn JH, Bierer SM, Bierer JA (2010) Modeling the electrode-neuron interface of cochlear implants: effects of neural survival, electrode placement, and the partial tripolar configuration. Hear Res 268:93–104

HACKER MJ, RATCLIFF R (1979) A revised table of d' for M-alternative forced choice. Percept Psychophys 26:168–170

HINOJOSA R, MARION M (1983) Histopathology of profound sensorineural deafness. Ann N Y Acad Sci 405:459–484

HUGHES ML (2008) A re-evaluation of the relation between physiological channel interaction and electrode pitch ranking in cochlear implants. J Acoust Soc Am 2008(124):2711–2714

HUGHES ML, ABBAS PJ (2006) The relation between electrophysiologic channel interaction and electrode pitch ranking in cochlear implant recipients. J Acoust Soc Am 119:1527–1537

JESTEADT W (1980) An adaptive procedure for subjective judgments. Atten Percept Psychophys 28:85–88

KWON BJ, VAN DEN HONERT C (2006) Effect of electrode configuration on psychophysical forward masking in cochlear implant listeners. J Acoust Soc Am 119:2994–3002

LANDSBERGER DM, PADILLA M, SRINIVASAN AG (2012) Reducing current spread using current focusing in cochlear implant users. Hear Res 284:16–24

LEE ER, FRIEDLAND DR, RUNGE CL (2012) Recovery from forward masking in elderly cochlear implant users. Otol Neurotol 33:355–363

LITVAK LM, SPAHR AJ, EMADI G (2007) Loudness growth observed under partially tripolar stimulation: model and data from cochlear implant listeners. J Acoust Soc Am 122:967–981

MENS LHM, BERENSTEIN CK (2005) Speech perception with mono- and quadrupolar electrode configurations: A crossover study. Otol Neurotol 26:957–964

PATTERSON RD (1976) Auditory filter shapes derived with noise stimuli. J Acoust Soc Am 59:640–654

SAOJI AA, LANDSBERGER DM, PADILLA M, LITVAK LM (2013) Masking patterns for monopolar and phantom electrode stimulation in cochlear implants. Hear Res 298:109–116

SHANNON RV, ZENG FG, KAMATH V, WYGONSKI J, EKELID M (1995) Speech recognition with primarily temporal cues. Science 270:303–304

SNEL-BONGERS J, BRIAIRE JJ, VANPOUCKE FJ, FRIJNS JH (2012) Spread of excitation and channel interaction in single- and dual-electrode cochlear implant stimulation. Ear Hear 33:367–376

SRINIVASAN AG, PADILLA M, SHANNON RV, LANDSBERGER DM (2013) Improving speech perception in noise with current focusing in cochlear implant users. Hear Res 299:29–36

TANG Q, BENITEZ R, ZENG FG (2011) Spatial channel interactions in cochlear implants. J Neural Eng 8:046029

UNDURRAGA JA, CARLYON RP, WOUTERS J, VAN WIERINGEN A (2012) Evaluating the noise in electrically evoked compound action potential measurements in cochlear implants. IEEE Trans Biomed Eng 59:1912–1923

VANPOUCKE FJ, ZAROWSKI AJ, PEETERS SA (2004) Identification of the impedance model of an implanted cochlear prosthesis from intracochlear potential measurements. IEEE Trans Biomed Eng 51:2174–2183

WU CC, LUO X (2013) Current steering with partial tripolar stimulation mode in cochlear implants. J Assoc Res Otolaryngol 14:213–231

WU CC, LUO X (2014) Electrode spanning with partial tripolar stimulation mode in cochlear implants. J Assoc Res Otolaryngol 15:1023–1036

ZHU Z, TANG Q, ZENG FG, GUAN T, YE D (2012) Cochlear-implant spatial selectivity with monopolar, bipolar and tripolar stimulation. Hear Res 283:45–58